THE JOURNAL OF PHYSICAL CHEMISTRY C

pubs.acs.org/JPCC Article

Pressure-Dependent Ion Rejection in Nanopores

Xin Zhang, Mingjie Wei,* Fang Xu, and Yong Wang*

Cite This: J. Phys. Chem. C 2020, 124, 20498−20505 Read Online

ACCESS | Metrics & More | Article Recommendations | Supporting Information

ABSTRACT: It is generally considered that ion rejection of a desalination membrane is independent of the operation pressure drops (ΔPs), which is typically not higher than 10 MPa. However, this may not be true for pressures as high as hundreds of megapascals usually used in simulations. Therefore, simulation results of high ΔPs cannot be directly used to predict real-world ion rejections, which is often overlooked. Herein, we investigate the ion rejection of carbon nanotube membranes in a large scale of ΔPs via nonequilibrium molecular dynamics simulations. With effective pressure drops (ΔP_e's) increased from 2.85 to 996 MPa, the ion rejection drops from 100% to nearly zero. Rather than directly investigating the rejection, the relationships of ion and water fluxes with ΔPs are separately investigated. With rising ΔP_es, the water flux increases linearly, while the ion flux undergoes a two-stage increase: first, an exponential increase at $\Delta P_e \leq 53.4$ MPa and then a linear increase. An equation describing the ΔP_e-dependent ion rejection is then developed based on these observations. Moreover, the rejection mechanism is also discovered, which indicates that the enhanced input energy makes ions easier to overcome the energy barrier rather than the molecular-configurational reasons. These findings are expected to fill the big gaps between simulations and experiments and may also be helpful for the rational design of the next-generation desalination membranes.

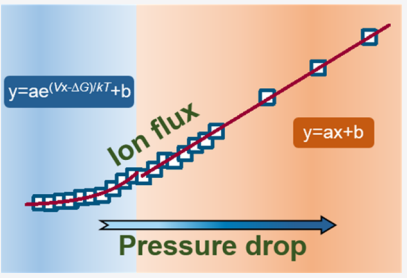

1. INTRODUCTION

The growing demand for freshwater is currently one of the major global issues. As an energy-efficient and cost-effective way, reverse osmosis (RO) technology can provide potable water to alleviate the water scarcity and is currently playing a dominating role in the desalination market.[1] However, the commonly used polymeric RO membranes have their own bottlenecks such as a trade-off effect between water permeance and salt rejection.[2] Thus, tremendous efforts were made to maximize the water permeance without sacrificing the salt rejection.[3] Usually, the drive to significantly enhance water permeance requires developments in new materials.[4]

The newly emerged nanomaterials with the angstrom-scale pores are alternatives for fabricating high-performance desalination membranes. Taking graphene oxide (GO) membranes as examples, there exists the ultrafast water transport through the confined channels. The extraordinary water permeation is attributed to the slip flow through the atomically smooth and unoxidized graphene channels.[5] Therefore, many efforts were made to fabricate the lamellar GO membranes for desalination.[6−8] Besides GO, it was found that fast water transport also exists in many other two-dimensional (2D) nanomaterials, such as molybdenum disulfide (MoS_2)[9] and hexagonal boron nitride (h-BN).[10] Because the unusual water flow under extreme confinement is beyond the classic continuum hydrodynamics, development in membranes using these nanomaterials as building blocks often needs guidance from molecular-level understandings.[11] However, the fluid transport through these membranes is hardly observed directly by existing experimental characterizations.

In the angstrom-scale confinement, nonequilibrium molecular dynamics (NEMD) simulations are practical and powerful techniques to simulate the pressure-driven membrane separation processes. By performing experiments on computers, it is feasible to make comprehensive understandings of transport properties, including both macroscopic behaviors of fluids (*e.g.*, flux) as well as molecular details of transport behaviors. By investigating the effects of pore size and chemical functionalization on desalination performance, Cohen-Tanugi and Grossman revealed that the nanoporous graphene enabled two to three orders of magnitudes higher water permeance than traditional RO membranes.[12] Compared to the nanoporous graphene, the water permeance of the single-layer MoS_2 nanopore was reported to be increased by ∼70% thanks to the hourglass geometry of nanopores.[13] Cao *et al.* reported that the water permeance of the 2D metal−organic framework was one order of magnitude higher than the nanoporous graphene or MoS_2.[14] Through NEMD simulations, many other membrane materials were reported to possess outstanding desalination performances, for example, GO,[15] graphyne,[16,17] and covalent organic framework (COF).[18]

However, the overwhelming majority of NEMD simulations use very high pressure drops (ΔPs), typically 100−1000 MPa,

Received: April 24, 2020
Revised: August 21, 2020
Published: August 25, 2020

https://dx.doi.org/10.1021/acs.jpcc.0c03641
J. Phys. Chem. C 2020, 124, 20498−20505

which is two to three orders of magnitude higher than the realistic operating pressures, which are typically 1−10 MPa.[12−14,19,20] Such a high-ΔP method was first proposed by Zhu *et al.* in 2002 and used to enhance the signal-to-noise ratio and the computational efficiency in the limited simulation time.[21] The prior computational work reported by Leung and Rempe investigated the effect of varying ΔPs on salt passage.[22] It was pointed out that the ion rejection would significantly decrease with increased ΔPs in nanoporous membranes. Unfortunately, the quantitative relationship between ion rejection and ΔP remains elusive. In most cases, the effect of ΔP on the ion rejection is overlooked. That is, the ion rejection in the high-ΔP simulation is directly regarded as that at experimentally low ΔP. In some works, the linear relationship between salt rejection and ΔP was assumed,[12,16,23] but this assumption is problematic because it does not have a solid theoretical basis. Cohen-Tanugi and Grossman used a rough kinetic model to qualitatively describe the decreased salt rejection with increased ΔPs.[12] Thomas and Corry reported that salt rejection would significantly decrease with enhanced ΔPs, and revealed that the 1.1 nm-wide carbon nanotube (CNT) with poor rejection in the high-ΔP simulation may afford the experimentally high ion rejection.[24] Therefore, the ion rejection from NEMD simulation results cannot accurately predict the experimental performance because of the vast difference in ΔPs.

Establishing the relationship of ion rejections with ΔPs and understanding the rejection mechanisms are of great significance to accurately assess the ion rejection performance from the NEMD simulation results. In this study, the CNT is chosen as the pore model because its nonpolar, inert, and smooth surface can exclude the possible adsorption of ions on pores, which is beneficial to analyze the mechanisms. The ion rejection performances of CNTs with various ΔPs from 10 to 1000 MPa are investigated via NEMD simulations. Because ion rejection is decided by water and ion fluxes, we develop equations to describe the effective pressure drop (ΔP_e)-dependent water and ion fluxes, and thus establish the relationship between ion rejection and ΔP_e. Such a relationship could extend to the lower ΔPs as the molecular mechanism of ion rejection at low ΔPs is also revealed.

2. SIMULATION DETAILS

2.1. Construction of Models. The snapshot for the NEMD simulation is shown in Figure 1. In the middle of the system is a CNT, which is enclosed by two graphene sheets with holes matching the CNT diameter. The simulation model also contains a feed chamber on the left and a permeate chamber on the right. Two rigid graphene sheets at the outer ends of the simulation box act as pistons to generate a pressure drop across the membrane, which pushes saline water across the CNT membrane. The feed chamber contains 58 Na^+ and 58 Cl^- solvated by 3242 water molecules, corresponding to the salt concentration of 1 mol L^{-1}. A higher salinity than that of seawater (0.599 mol L^{-1}) is used to collect sufficient statistics of ion transport events within the limited simulation time, which is commonly used in simulation works.[13,14,25] The permeate chamber contains 607 water molecules. The x and y dimensions of the simulation system are set to 3.19 and 3.40 nm, respectively. (10, 10) armchair CNT was selected with an effective diameter of 1.01 nm, after deducting the van der Waals diameter of carbon atom (0.34 nm). The effective diameter of 1.01 nm is slightly wider than the one that achieves a complete rejection at 100 MPa,[26] promising the sensitivity of ion rejection to ΔPs. The length of the CNT is set to 2.34 nm, under which the ion rejection may decrease with the length.[26]

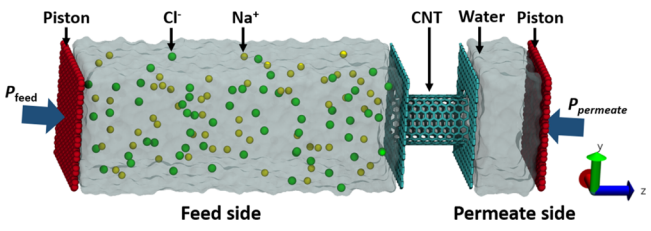

Figure 1. Modeling of the simulations. Snapshot of the simulated water and ion transport through the CNT membrane. The compositions are labeled in the figure.

2.2. Simulation Protocol. All of the simulations were conducted with the LAMMPS package.[27] All carbon atoms were held rigid. Fixed membranes can prevent the deformation of membranes caused by the pressure, which is widely used in many simulations.[14,25,28] The atom interactions included both the 12-6 Lennard-Jones (LJ) and the Coulombic interactions. The SPC/E water model was used with the SHAKE algorithm that constrains the bonds and angles. Correspondingly, the parameters for Na^+ and Cl^- were proposed by Joung and Cheatham.[29] The LJ interactions between carbon and oxygen atoms were selected as the parameters: σ_{C-O} = 0.319 nm, ε_{C-O} = 0.392 kJ mol^{-1}.[30] Lorentz−Berthelot combination rules were employed to generate LJ cross-interaction parameters between different elements. The cutoff distances of LJ potentials and electrostatic interactions were set to 1.0 and 1.2 nm, respectively. Long-range electrostatic interactions were computed by the particle−particle particle-mesh method with the accuracy of 10^{-4}.[31] Periodic boundary conditions were only applied in x and y dimensions.

For each simulation, energy minimization was first conducted with a tolerance of 10^{-5}. Then, 5 ns equilibrium molecular dynamics simulation was performed at 300 K and 0.1 MPa to allow water molecules to wet CNT membranes. Finally, in the NEMD simulations, the pressure drop (ΔP) across the membrane was generated as

$$\Delta P = P_{\text{feed}} - P_{\text{permeate}} \tag{1}$$

where P_{feed} and P_{permeate} represent the pressures on the feed and permeate pistons, respectively. P_{feed} was set to the desired pressure, and P_{permeate} was set to 0.1 MPa (ambient pressure). To generate the desired pressures, the external forces were applied to the atoms of the piston, which can be calculated as

$$f = \frac{PA}{n} \tag{2}$$

where A is the cross-sectional area of the membrane and n is the number of carbon atoms of the piston. The temperature of the system was kept at 300 K with a Nosé−Hoover thermostat. The trajectories were saved every 1 ps with a time step of 1 fs. The ΔP ranging from 10 to 1000 MPa was used. Based on the magnitude of the ΔP, the simulation time is ranged from 1 to 300 ns so as to allow half number of the water molecules (~1600) in feed chambers to permeate through the membrane at each ΔP. To reduce the statistical deviation, the results were calculated by averaging over three separate runs with different sets of initial configurations.

https://dx.doi.org/10.1021/acs.jpcc.0c03641
J. Phys. Chem. C 2020, 124, 20498−20505

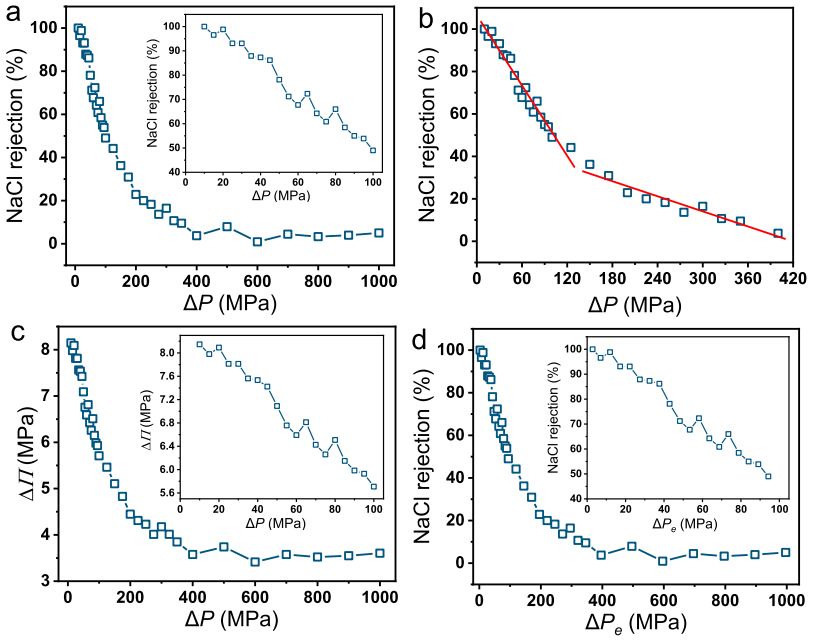

Figure 2. ΔP-dependent NaCl rejection. (a) NaCl rejection as a function of ΔPs ranging from 10 to 1000 MPa. (b) Linear relationship between NaCl rejection and ΔP in two short periods of ΔPs from 10 to 125 MPa and from 150 to 400 MPa. (c) Osmotic pressure difference ($\Delta\Pi$) as a function of ΔPs. (d) NaCl rejection as a function of effective pressure drops (ΔP_e's) from 2.85 to 996 MPa. Insets for (a,c,d) are zoomed in 0−105 MPa.

2.3. Post-Simulation Analysis. As shown in Figure S1, the number of water molecules permeated through the CNT membrane increases linearly with the sampling time, which means that the water flow is in a steady state. The water flux was calculated by the slope of the number of water molecules permeated through the membrane with the sampling time (Figure S1). Besides, ion rejection (R) is defined as

$$R = 1 - \frac{c_p}{c_f} \tag{3}$$

where c_p and c_f represent the ion concentrations in the permeate and feed sides, respectively. Herein, R = 100% means that only water molecules can pass through the membrane, while R = 0% means that the ion concentration of the permeate solution is equal to that of the initial feed solution. Based on $c_p = F_i/F_w$ and $c_f = n_i/n_w$, R can be calculated in a detailed expression as below

$$R = 1 - \frac{F_i/F_w}{n_i/n_w} \tag{4}$$

where F_i and F_w are water and ion fluxes, respectively. The number of ions and water passing through the membrane during a span of simulation time was counted to calculate F_i and F_w. n_i and n_w are the initial number of ions and water molecules in the feed side, which is equal to 58 and 3242, respectively. Obviously, ion rejection is dependent on F_i and F_w. Therefore, in order to establish the relationship between ion rejection and ΔP, the relationships of F_i and F_w with ΔPs are investigated in the following analysis.

3. RESULTS AND DISCUSSION

3.1. Dependence of Ion Rejection on ΔPs. We first investigate NaCl rejection with ΔP ranging from 10 to 1000 MPa. As shown in Figure 2a, the ion rejection is highly dependent on the applied ΔPs. When ΔP decreases from 1000 to 400 MPa, the ion rejection maintains ∼4%. When ΔP decreases from 400 to 10 MPa, the ion rejection will increase gradually from 4 to 100%. To accurately describe the ΔP-dependent ion rejections, the intervals of ΔPs are smaller when the changes of ion rejections are faster, which are 5, 25, and 100 MPa with ΔPs of 10−100, 100−350, and 400−1000 MPa, respectively. Enhanced ion rejections with decreased ΔPs were also reported in many other materials, for example, graphene,[12] graphyne,[16] and COFs,[32] the staking layered structure of which afford one-dimensional straight pores such as CNTs.

In NEMD simulations, the ΔP of 100 MPa is often used,[12−14] and the corresponding ion rejection is 49%. This result indicates that the 1.01 nm-wide CNT membrane is undesirable for desalination. However, if the ΔP is 10 MPa, which is near to the usual experimental or industrial operation condition,[33] the ion rejection is as high as 100%, which is absolutely desirable for desalination. Therefore, the results of high-ΔP simulations are not reliable to predict the ion rejection performances.

The findings from high-ΔP simulations will underestimate the experimental ion rejection performance. In other words, a wider nanopore with poor rejection at high ΔP may also be desirable for desalination because its ion rejection performance is much better at low ΔP. For example, the previously reported maximum diameter for complete salt rejection of CNTs is 0.88 nm at 100 MPa.[26] If the pore diameter increases from 0.88 to 1.01 nm, the NaCl rejections are all 100% at experimental operation conditions. However, the water permeance of the 1.01 nm-wide CNT is dramatically increased from 545.6 to 1270 L m^{-2} h^{-1} bar^{-1} compared to the 0.88 nm-wide CNT. Therefore, the underestimation will of course mislead the design of new membranes.

Because the effect of ΔP on the ion rejection is pronounced, it is important to figure out the origin of this observation and to develop an equation to describe the ΔP-dependent ion rejection. As it is widely assumed a linear relationship in the

https://dx.doi.org/10.1021/acs.jpcc.0c03641
J. Phys. Chem. C 2020, 124, 20498−20505

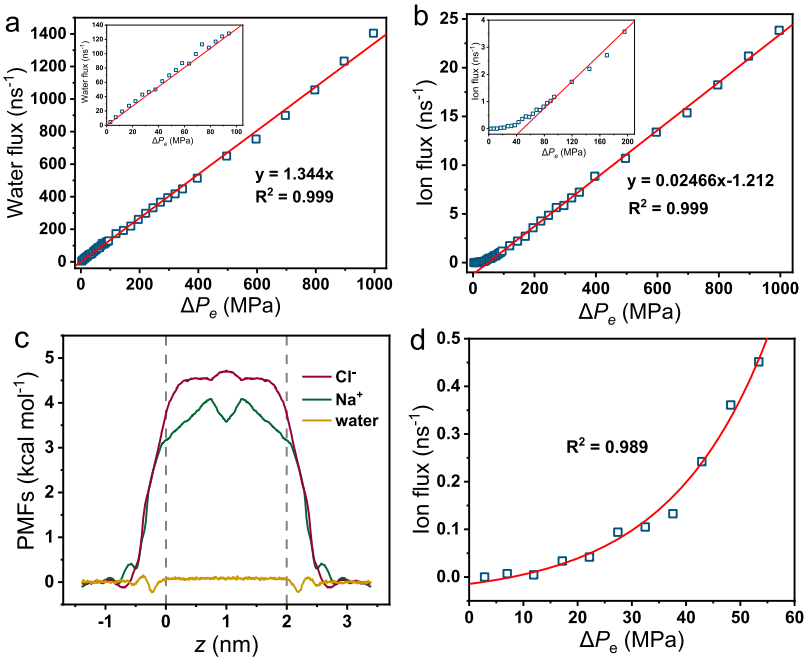

Figure 3. Water and ion fluxes with the relationship of ΔP_e's. (a) Water flux as a function of ΔP_e's ranging from 2.85 to 996 MPa. The inset is zoomed in 0−105 MPa. (b) Ion flux as a function of ΔP_e ranging from 2.85 to 996 MPa. The linear fitting is only applied to 58.2−996 MPa. The inset is zoomed in 0−210 MPa. (c) PMFs for Cl^-, Na^+, and water molecules passing through the CNT membrane. The two gray dashed lines denote the positions of the entrance and exit of the membrane. (d) Ion flux as a function of ΔP_e ranging from 2.85 to 53.4 MPa. Equation 9 is used to fit the data.

literature,[12,14,16] we try to use this relationship to fit the data. As shown in Figure 2b, the likely linear relationship is only observed in two short periods of ΔPs of 10−125 and 150−400 MPa. Obviously, the linear relationship cannot fit the data well in the whole range of ΔPs.

It is well-known that the applied ΔP is directly affected by the osmotic pressure difference ($\Delta\Pi$). $\Delta\Pi$ originated from the ionic concentration difference should be deducted from ΔP. The previous study using the same force fields of water and ion as our simulations showed that the calculated osmotic pressure is highly consistent with experiments and the van't Hoff equation at NaCl concentrations below 2 mol L^{-1}.[34] Therefore, $\Delta\Pi$ is calculated by the van't Hoff equation and the calculation details are shown in the Supporting Information. As shown in Figure 2c, with ΔP decreased from 1000 to 400 MPa, $\Delta\Pi$ maintains around 3.57 MPa. When ΔP decreases from 400 to 10 MPa, $\Delta\Pi$ is sharply increased from 3.57 to 8.15 MPa. The effect of $\Delta\Pi$ on ΔP is significant at low ΔPs, but negligible at high ΔPs. $\Delta\Pi$ is highly dependent on salt rejection because a higher salt rejection will lead to a higher concentrated solution of the feed side in a limited simulation box. It should be noted that the calculated $\Delta\Pi$s are much higher than that in experiments for two reasons. First, the initial salt concentration of 1 mol L^{-1} in the feed side is much higher than that commonly used in experiments (~0.0342 mol L^{-1}).[33] The other reason is that the limited simulation box will increase the concentration difference, especially when the rejection is high. In addition, the above-calculated $\Delta\Pi$ is the average value during the filtration process. The instantaneous $\Delta\Pi$ can reach a maximum of 10 MPa at the concentration difference of 2 mol L^{-1}, which is equal to the applied minimum ΔP of 10 MPa. In this situation, we find that at most half of the water molecules in the feed chamber are permeated through the membrane, which is nearly independent of the sampling time. Therefore, to accurately calculate the water and ion fluxes, we collect the data during 40% of water molecules in the feed chamber permeated through the membrane at the ΔP of 10 MPa.

To exclude the effect of $\Delta\Pi$ on ΔP, the effective pressure drop (ΔP_e) is defined as

$$\Delta P_e = \Delta P - \Delta\Pi \tag{5}$$

In order to overcome $\Delta\Pi$s, the ΔPs used in this work are higher than 10 MPa. Therefore, the minimum of the effective pressure drop (ΔP_e) is in the range of the experimental operations. As ΔP increases from 10 to 1000 MPa, ΔP_e is increased from 2.85 to 996 MPa. As shown in Figure 2d, the relationship between ion rejection and ΔP_e is nearly unchanged compared to ΔP. It is also difficult to find a direct relationship between ion rejection and ΔP_e. From eq 4, it is obvious that ion rejection is decided by the water flux (F_w) and the ion flux (F_i). We then investigate F_w and F_i with the relationship of ΔP_e's.

3.2. Dependence of Water and Ion Fluxes on ΔPs.

Water flux as a function of ΔP_e's is shown in Figure 3a. As expected from the continuum hydrodynamics, there is a finely linear and zero-axial relationship between water flux and ΔP_e as shown below

$$F_w = 1.344\Delta P_e \tag{6}$$

Although the classical continuum hydrodynamics is not sufficiently reasonable to explain the behaviors of water under extreme confinement,[35] this empirical linear relationship was previously reported.[36−38] Based on this linear relationship, the high-ΔP_e water flux can be extrapolated to the low-ΔP_e water flux.

After establishing the relationship between F_w and ΔP_e, we then try to figure out the relationship between F_i and ΔP_e. As

https://dx.doi.org/10.1021/acs.jpcc.0c03641
J. Phys. Chem. C 2020, 124, 20498−20505

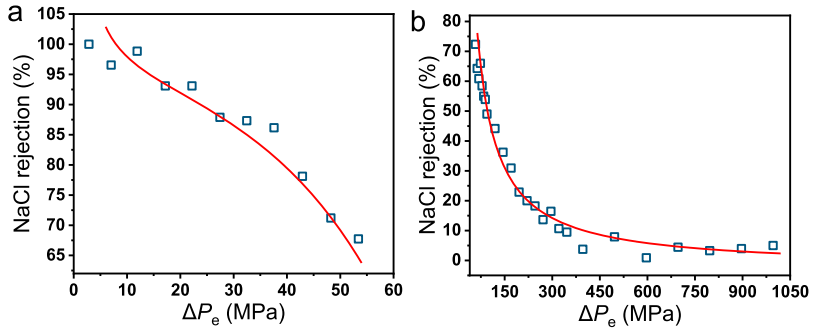

Figure 4. Relationship between ion rejection and ΔP_e: (a) ΔP_e from 2.85 to 53.4 MPa; (b) ΔP_e from 58.2 to 996 MPa. The blue symbols are the simulation data, and the red curves are plotted by eq 11.

shown in Figure 3b, F_i shows a monotonic increase with ΔP_e increased from 2.85 to 996 MPa. Similar to F_w, there seems a linear increase in F_i with ΔP_e. The linear relationship is sufficiently reasonable to describe F_i with ΔP_e from 58.2 to 996 MPa. It is found that the magnitude of F_i is much less than that of F_w because the ion concentration is much lower than the water concentration.

However, as shown in the inset of Figure 3b, when ΔP_e is <58.2 MPa, F_i decreases slower and drifts away from the linearly fitted line. In this period of ΔP_e, there should be another relationship. Based on the Arrhenius model, eq 7 is often assumed to describe F_i as it is in direct proportion to the reaction rate constant.[12,39,40]

$$F_i \propto e^{-\Delta G/kT} \tag{7}$$

where ΔG is the free energy barrier for ion passing through the membrane, k is the Boltzmann's constant of 1.381×10^{-23} J K^{-1}, and T is the liquid temperature of 300 K. From eq 7, F_i is only dependent on ΔG, and a higher ΔG will lead to a smaller F_i, and vice versa. The magnitude of ΔG is obtained from the potential of mean force (PMF). The calculation details of PMF are shown in the Supporting Information. As shown in Figure 3c, the ΔG for Cl^- of 4.72 kcal mol^{-1} is higher than that for Na^+ of 4.09 kcal mol^{-1}. This observation is because a larger hydration shell of Cl^- has to peel off more water molecules while entering nanopores compared to Na^+. Because of the higher energy barrier for Cl^-, Cl^- is easier to be retained than Na^+. Once Cl^- is rejected, the oppositely charged ion of Na^+ will be simultaneously rejected to maintain the charge balance. Therefore, NaCl rejection is decided by Cl^- rejection. In the following discussions, we will further investigate the relationship between F_i and ΔP_e based on the data of Cl^-.

Besides ΔG, the input energy (E_i) will also influence ion transport, which can be calculated as

$$E_i = V_i \Delta P_e \tag{8}$$

where V_i is the effective volume of the hydrated ion. From the radial distribution functions (RDFs) of ions with oxygen atoms of water in Figure S3, the peaks and valleys indicate the formation of the hydration shells, and the hydrated ion can be regarded as a sphere. The radii of the hydrated Cl^- is 3.775 Å, and thus V_i is calculated as 225.3 $Å^3$. Obviously, E_i increases linearly with rising ΔP_e, while ΔG is a constant value. Driven by the increased E_i, F_i will increase with rising ΔP_e (Figure 3b). Taking both ΔG and E_i into consideration, we can transform eq 7 into a detailed expression as below

$$F_i = A_0\, e^{(V_i \Delta P_e - \Delta G)/kT} + F_0 \tag{9}$$

where F_0 and A_0 are set to the fitted parameters. The exponential decrease of F_i with ΔP_e decreased from 53.4 to 2.85 MPa is finely fitted in Figure 3d by using eq 9, and F_0 and A_0 are calculated as −0.04182 and 74.38.

In general, as shown in eq 10, F_i undergoes first an exponential increase with ΔP_e increased from 2.85 to 53.4 MPa and then a linear increase with ΔP_e further increased to 996 MPa.

$$F_i = \begin{cases} 74.38\, e^{0.05440\Delta P_e - 7.914} - 0.04182 & \Delta P_e \le 53.4 \\ 0.02466\Delta P_e - 1.212 & \Delta P_e > 53.4 \end{cases} \tag{10}$$

From eq 10, there is a threshold ΔP_e where F_i transforms from an exponential increase to a linear increase. The threshold ΔP_e may be determined by both ΔG and E_i. When ΔP_e is smaller than 53.4 MPa, the calculated E_i is smaller than 1.73 kcal mol^{-1} based on eq 8, which is much smaller than the ΔG of 4.72 kcal mol^{-1}. In this situation, ΔG plays a dominating role, and thus the modified Arrhenius model as eq 9 can describe the relationship between F_i and ΔP_e. With further increased E_i, it shows a linear relationship between F_i and ΔP_e.

3.3. Description of ΔP-Dependent Ion Rejections.

By introducing eqs 6 and 10 that describe ΔP_e-dependent F_i and F_w into eq 4, the relationship between ion rejection and ΔP_e can be described as

$$R = \begin{cases} 1 + \dfrac{1.739 - 3093\, e^{0.05440\Delta P_e - 7.914}}{\Delta P_e} & \Delta P_e \le 53.4 \\ \dfrac{50.41}{\Delta P_e} - 0.026 & \Delta P_e > 53.4 \end{cases} \tag{11}$$

The curves of describing ΔP_e-dependent ion rejection based on eq 11 and the simulation data are shown in Figure 4a,b. When ΔP_e is smaller than 53.4 MPa, the relationship between ion rejection and ΔP_e is complicated. Because eq 11 is based on the fittings of ion and water fluxes, it neglects the boundary condition, that is, the ion rejection will slightly exceed 100% (the upper limit of rejection) at $\Delta P_e \le \sim 7$ MPa. When ΔP_e is larger than 53.4 MPa, the inversely proportional relationship is sufficiently reasonable to describe the ion rejection. With increased ΔP_e's, the ion rejection shows a monotonic decrease and the decreasing rate slows down. When ΔP_e is larger than 396 MPa (ΔP = 400 MPa), ion rejection is slightly decreased with rising ΔP_e based on eq 11, which is consistent with the nearly unchanged ion rejection from simulation results. The applied ΔP is typically considered to be no larger than 1000 MPa because water will exist as ice beyond this value based on

https://dx.doi.org/10.1021/acs.jpcc.0c03641
J. Phys. Chem. C 2020, 124, 20498−20505

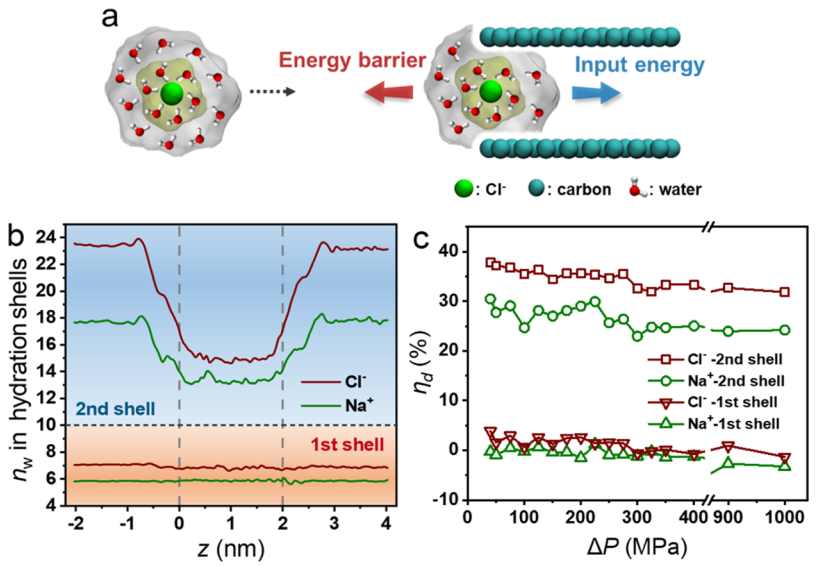

Figure 5. Behaviors of ion transport in nanopores. (a) Schematic illustrations of the hydrated Cl^- with two hydration shells in bulk aqueous solutions (left) and the partially dehydrated Cl^- at the entrance of CNTs (right). When the partially dehydrated Cl^- is ready to enter the nanopore, the energy barrier pulls it to return to the bulk aqueous solution, while the input energy pushes it into the nanopore at the same time. Atomic colors: carbon, cyan; Cl^-, green. The light yellow and grey shadings denote the first and second hydration shells of ions, respectively. The two grey dashed lines represent the entrance and exit of the CNT. (b) Profiles of the average number of water molecules (n_w) inside the first and second hydration shells of Cl^- and Na^+ along the z direction at 100 MPa. The light organic and blue shadings denote the first and second hydration shells, respectively. (c) Dehydration degree (η_d) of Cl^- and Na^+ as a function of ΔPs.

the experimental phase diagram.[41] In general, the ion rejection shows a piecewise function of ΔP_e's, which replicates the observed behaviors well. Only when ΔP_e is smaller than 53.4 MPa, it can be extrapolated from high to low ΔP_e. Otherwise, the ion rejection at very high ΔP_e cannot be extrapolated to the realistic low ΔP_e. Besides, by introducing eq 11 into eq 5, the relationship between ion rejection and ΔP can be established after taking $\Delta\Pi$ into consideration.

3.4. Molecular Mechanisms of ΔP-Dependent Ion Rejections. After developing an equation to describe the ΔP-dependent ion rejections, it is also important to figure out the mechanisms from molecular observations. There have been four rejection mechanisms in nanopore separation, which includes (1) molecular sieve; (2) electrostatic repulsion; (3) dehydration barrier; (4) in-pore transport difference.[42,43] As illustrated in our previous studies, the mechanisms of both molecular sieve and electrostatic repulsion can be excluded in inert and neutral CNT pores.[26] The in-pore transport difference is also negligible in nonpolar nanopores such as CNTs.[43] Therefore, the dehydration barrier may play an important role in ion rejections.[42,44−46]

The hydration size of ions can be obtained as the minimums of the RDF curves in Figure S3. The second hydration diameters of Cl^- and Na^+ are calculated as 1.21 and 1.09 nm, respectively, both of which are larger than the 1.01 nm of the CNT diameter. Therefore, the hydrated ions have to peel off some hydrating water molecules while entering CNT pores (Figure 5a). To observe the process of ion dehydration, the profiles of the average number of water molecules (n_w) inside the first and second hydration shell of Cl^- and Na^+ at 100 MPa are shown in Figure 5b. n_w in the first hydration shell of ions is constant because the first hydration diameters of ions (Na^+: 0.64 nm, Cl^-: 0.76 nm) are smaller than the CNT diameter. However, n_w in the second hydration shell is sharply decreased when an ion enters the nanopore and recovers when an ion leaves the nanopore. The dehydration of the second hydration shells is the origin of the energy barrier for ions. Besides, the hydrated Cl^- loses more hydrating water molecules than the Na^+ does, which results in a higher energy barrier for Cl^- (Figure 3c). Moreover, it should be noted that the ion rejection is determined by not only the pore size but also the membrane hydrophilicity. A hydrophilic membrane with a pore diameter of ∼0.8 nm often has moderate rejections to ions because the atoms of the pore wall (oxygen, nitrogen, hydrogen, or some other atoms) will compensate for the hydration loss of ions, which lowers the energy barrier for ion passage.[43] In this study, the hydrophobic CNT pore with a diameter of 1.01 nm has very high rejections at low ΔPs because only the dehydration barrier takes effect on the ion rejection, which is consistent with the reported literature.[24]

We then investigate the effect of ΔP on ion dehydration. Herein, the dehydration degree (η_d) of ions is defined as

$$\eta_d = 1 - \frac{n_p}{n_b} \tag{12}$$

where n_p and n_b are the average number of water molecules inside the hydration shells of ions in the middle of nanopores (z = 0.6−1.4 nm) and in the bulk aqueous solutions. Figure 5c shows η_d of the first and second hydration shells of ions as a function of ΔPs. It is found that η_d of both first and second hydration shell of ions is nearly unchanged with ΔPs, indicating that the dehydration process is nearly independent of ΔPs. The oscillation of η_d in the second hydration shell is because a higher rejection at a lower ΔP will result in fewer ions entering nanopores. With a complete rejection, no ion enters the nanopore, and thus the dehydration process cannot be observed. After all, as ΔP does not change the membrane properties and thermodynamic state of ion dehydration, the dehydration mechanism cannot explain the ΔP-dependent ion rejections either.

https://dx.doi.org/10.1021/acs.jpcc.0c03641
J. Phys. Chem. C 2020, 124, 20498−20505

We then focus on the energy analysis rather than the molecular structure. Ion dehydration is commonly regarded as the origin of the energy barrier for ion transport through inert nanopores.[46] Similar to ion dehydration, water molecules have to rearrange hydrogen bonds to enter CNTs,[37,47] which is the origin of the energy barrier for water transport. As shown in Figure 3c, the energy barrier for water molecules is much lower than that for ions. Therefore, the high rejections are observed at relatively low ΔPs. Besides the effect of the energy barrier, the movement of the partially dehydrated Cl^- is also decided by the input energy (Figure 5a). With increased ΔP_e's, the higher input energy makes ions easier to overcome the energy barrier, which consequently decreases ion rejections. When the input energy is very large compared to the difference in the energy barrier between ions and water molecules, ions can pass through nanopores easily, and the ion rejection is nearly zero.

It should be noted that the molecular structure of ion transport does not change with the declining ΔP_e. Hence, eq 9 will work at a lower ΔP_e of experimental operations. We believe that eq 11 will be valid for predicting the ion rejection performance at the experimental operating conditions.

4. CONCLUSIONS

In summary, we investigate the effect of pressure drop (ΔP) on ion rejection via NEMD simulations. In the 1.01 nm-wide and 2.34 nm-long CNT membrane, it is found that the ion rejection is decreased from 100 to ∼4% with ΔP increased from 10 to 1000 MPa. Because ion rejection performance is dependent on ion and water fluxes, the effects of ΔP on ion and water fluxes are separately investigated. The effective pressure drops (ΔP_e's) rather than ΔPs are used to exclude the effect of the osmotic pressure differences. ΔP_e ranges from 2.85 to 996 MPa, which covers the experimental observations. It is found that the water flux is increased linearly with ΔP_e, whereas the ion flux undergoes first an exponential increase at $\Delta P_e \leq 53.4$ MPa and then a linear increase if ΔP_e further increases to 996 MPa. Considering both the water and ion fluxes, we propose an equation to describe the ΔP_e-dependent ion rejection. Moreover, the rejection mechanism is revealed. The ion rejection drops with rising ΔP_e's because the enhanced input energy makes ions easier to overcome the energy barrier. These findings warn us to consider the effect of ΔP on the ion rejection while using very high ΔPs in simulations. With our proposed equations and the revealed rejection mechanisms, it will be helpful to make a reliable prediction of the experimental ion rejection performance.

■ ASSOCIATED CONTENT

Supporting Information

The Supporting Information is available free of charge at https://pubs.acs.org/doi/10.1021/acs.jpcc.0c03641.

Illustration of steady-state flows; calculation details of osmotic pressure differences ($\Delta\Pi$s); calculation details of PMFs; RDFs; and simulation results for the enlarged simulation box (PDF)

■ AUTHOR INFORMATION

Corresponding Authors

Mingjie Wei − *State Key Laboratory of Materials-Oriented Chemical Engineering, and College of Chemical Engineering, Nanjing Tech University, Nanjing 211816, Jiangsu, P. R. China;* orcid.org/0000-0001-7601-4749; Phone: +86-25-83172247; Email: mj.wei@njtech.edu.cn; Fax: +86-25-83172292

Yong Wang − *State Key Laboratory of Materials-Oriented Chemical Engineering, and College of Chemical Engineering, Nanjing Tech University, Nanjing 211816, Jiangsu, P. R. China;* orcid.org/0000-0002-8653-514X; Email: yongwang@njtech.edu.cn

Authors

Xin Zhang − *State Key Laboratory of Materials-Oriented Chemical Engineering, and College of Chemical Engineering, Nanjing Tech University, Nanjing 211816, Jiangsu, P. R. China*

Fang Xu − *State Key Laboratory of Materials-Oriented Chemical Engineering, and College of Chemical Engineering, Nanjing Tech University, Nanjing 211816, Jiangsu, P. R. China*

Complete contact information is available at: https://pubs.acs.org/10.1021/acs.jpcc.0c03641

Notes

The authors declare no competing financial interest.

■ ACKNOWLEDGMENTS

Financial support from the National Key Research and Development Program of China (2017YFC0403902), the National Science Fund for Distinguished Young Scholars (21825803), the Jiangsu Natural Science Foundations (BK20190085), and the Postgraduate Research & Practice Innovation Program of Jiangsu Province (KYCX20_1028). We thank the High Performance Computing Center of Nanjing Tech University for supporting the computational resources. We are also grateful to the Program of Excellent Innovation Teams of Jiangsu Higher Education Institutions and the Project of Priority Academic Program Development of Jiangsu Higher Education Institutions (PAPD).

■ REFERENCES

(1) Ghaffour, N.; Missimer, T. M.; Amy, G. L. Technical Review and Evaluation of the Economics of Water Desalination: Current and Future Challenges for Better Water Supply Sustainability. *Desalination* **2013**, *309*, 197−207.

(2) Geise, G. M.; Park, H. B.; Sagle, A. C.; Freeman, B. D.; McGrath, J. E. Water Permeability and Water/Salt Selectivity Tradeoff in Polymers for Desalination. *J. Membr. Sci.* **2011**, *369*, 130−138.

(3) Park, H. B.; Kamcev, J.; Robeson, L. M.; Elimelech, M.; Freeman, B. D. Maximizing the Right Stuff: The Trade-Off between Membrane Permeability and Selectivity. *Science* **2017**, *356*, No. eaab0530.

(4) Werber, J. R.; Osuji, C. O.; Elimelech, M. Materials for Next-Generation Desalination and Water Purification Membranes. *Nat. Rev. Mater.* **2016**, *1*, 16018.

(5) Nair, R. R.; Wu, H. A.; Jayaram, P. N.; Grigorieva, I. V.; Geim, A. K. Unimpeded Permeation of Water Through Helium-Leak-Tight Graphene-Based Membranes. *Science* **2012**, *335*, 442−444.

(6) Joshi, R. K.; Carbone, P.; Wang, F. C.; Kravets, V. G.; Su, Y.; Grigorieva, I. V.; Wu, H. A.; Geim, A. K.; Nair, R. R. Precise and Ultrafast Molecular Sieving through Graphene Oxide Membranes. *Science* **2014**, *343*, 752−754.

(7) Sun, P.; Wang, K.; Zhu, H. Recent Developments in Graphene-Based Membranes: Structure, Mass-Transport Mechanism and Potential Applications. *Adv. Mater.* **2016**, *28*, 2287−2310.

(8) Abraham, J.; Vasu, K. S.; Williams, C. D.; Gopinadhan, K.; Su, Y.; Cherian, C. T.; Dix, J.; Prestat, E.; Haigh, S. J.; Grigorieva, I. V.; Carbone, P.; Geim, A. K.; Nair, R. R. Tunable Sieving of Ions Using Graphene Oxide Membranes. *Nat. Nanotechnol.* **2017**, *12*, 546−550.

(9) Li, H.; Ko, T.-J.; Lee, M.; Chung, H.-S.; Han, S. S.; Oh, K. H.; Sadmani, A.; Kang, H.; Jung, Y. Experimental Realization of Few Layer Two-Dimensional Mos2 Membranes of near Atomic Thickness for High Efficiency Water Desalination. *Nano Lett.* **2019**, *19*, 5194−5204.
(10) Pendse, A.; Cetindag, S.; Lin, M. H.; Rackovic, A.; Debbarma, R.; Almassi, S.; Chaplin, B. P.; Berry, V.; Shan, J. W.; Kim, S. Charged Layered Boron Nitride-Nanoflake Membranes for Efficient Ion Separation and Water Purification. *Small* **2019**, *15*, 1904590.
(11) Wang, J.; Zhu, J.; Zhang, Y.; Liu, J.; Van der Bruggen, B. Nanoscale Tailor-Made Membranes for Precise and Rapid Molecular Sieve Separation. *Nanoscale* **2017**, *9*, 2942−2957.
(12) Cohen-Tanugi, D.; Grossman, J. C. Water Desalination across Nanoporous Graphene. *Nano Lett.* **2012**, *12*, 3602.
(13) Heiranian, M.; Farimani, A. B.; Aluru, N. R. Water Desalination with a Single-Layer MoS_2 Nanopore. *Nat. Commun.* **2015**, *6*, 8616.
(14) Cao, Z.; Liu, V.; Barati Farimani, A. Water Desalination with Two-Dimensional Metal-Organic Framework Membranes. *Nano Lett.* **2019**, *19*, 8638−8643.
(15) Lin, L.-C.; Grossman, J. C. Atomistic Understandings of Reduced Graphene Oxide as an Ultrathin-Film Nanoporous Membrane for Separations. *Nat. Commun.* **2015**, *6*, 8335.
(16) Kou, J.; Zhou, X.; Lu, H.; Wu, F.; Fan, J. Graphyne as the Membrane for Water Desalination. *Nanoscale* **2014**, *6*, 1865−1870.
(17) Zhu, C.; Li, H.; Zeng, X. C.; Wang, E.; Meng, S. Quantized Water Transport: Ideal Desalination through Graphyne-4 Membrane. *Sci. Rep.* **2013**, *3*, 3163.
(18) Lin, L.-C.; Choi, J.; Grossman, J. C. Two-Dimensional Covalent Triazine Framework as an Ultrathin-Film Nanoporous Membrane for Desalination. *Chem. Commun.* **2015**, *51*, 14921−14924.
(19) Borg, M. K.; Lockerby, D. A.; Ritos, K.; Reese, J. M. Multiscale Simulation of Water Flow through Laboratory-Scale Nanotube Membranes. *J. Membr. Sci.* **2018**, *567*, 115−126.
(20) Ritos, K.; Borg, M. K.; Mottram, N. J.; Reese, J. M. Electric Fields Can Control the Transport of Water in Carbon Nanotubes. *Philos. Trans. R. Soc., A* **2016**, *374*, 20150025.
(21) Zhu, F.; Tajkhorshid, E.; Schulten, K. Pressure-Induced Water Transport in Membrane Channels Studied by Molecular Dynamics. *Biophys. J.* **2002**, *83*, 154−160.
(22) Leung, K.; Rempe, S. B. Ion Rejection by Nanoporous Membranes in Pressure-Driven Molecular Dynamics Simulations. *J. Comput. Theor. Nanosci.* **2009**, *6*, 1948−1955.
(23) Cohen-Tanugi, D.; Lin, L.-C.; Grossman, J. C. Multilayer Nanoporous Graphene Membranes for Water Desalination. *Nano Lett.* **2016**, *16*, 1027−1033.
(24) Thomas, M.; Corry, B. A Computational Assessment of the Permeability and Salt Rejection of Carbon Nanotube Membranes and Their Application to Water Desalination. *Philos. Trans. R. Soc., A* **2016**, *374*, 20150020.
(25) Yan, Y. G.; Wang, W. S.; Li, W.; Loh, K. P.; Zhang, J. A Graphene-Like Membrane with an Ultrahigh Water Flux for Desalination. *Nanoscale* **2017**, *9*, 18951−18958.
(26) Zhang, X.; Wei, M.; Xu, F.; Wang, Y. Thickness-Dependent Ion Rejection in Nanopores. *J. Membr. Sci.* **2020**, *601*, 117899.
(27) Plimpton, S. Fast Parallel Algorithms for Short-Range Molecular Dynamics. *J. Comput. Phys.* **1995**, *117*, 1−19.
(28) Heiranian, M.; Aluru, N. R. Nanofluidic Transport Theory with Enhancement Factors Approaching One. *ACS Nano* **2020**, *14*, 272−281.
(29) Joung, I. S.; Cheatham, T. E. Determination of Alkali and Halide Monovalent Ion Parameters for Use in Explicitly Solvated Biomolecular Simulations. *J. Phys. Chem. B* **2008**, *112*, 9020−9041.
(30) Werder, T.; Walther, J. H.; Jaffe, R. L.; Halicioglu, T.; Koumoutsakos, P. On the Water−Carbon Interaction for Use in Molecular Dynamics Simulations of Graphite and Carbon Nanotubes. *J. Phys. Chem. B* **2003**, *107*, 1345−1352.
(31) Darden, T.; York, D.; Pedersen, L. Particle mesh Ewald: AnN·log(N) method for Ewald sums in large systems. *J. Chem. Phys.* **1993**, *98*, 10089−10092.
(32) Wei, M.; Zhou, W.; Xu, F.; Wang, Y. Nanofluidic Behaviors of Water and Ions in Covalent Triazine Framework (CTF) Multilayers. *Small* **2019**, *16*, 1903879.
(33) Qasim, M.; Badrelzaman, M.; Darwish, N. N.; Darwish, N. A.; Hilal, N. Reverse Osmosis Desalination: A State-of-the-Art Review. *Desalination* **2019**, *459*, 59−104.
(34) Smith, W. R.; Moučka, F.; Nezbeda, I. Osmotic Pressure of Aqueous Electrolyte Solutions Via Molecular Simulations of Chemical Potentials: Application to Nacl. *Fluid Phase Equilib.* **2016**, *407*, 76−83.
(35) Thomas, J. A.; McGaughey, A. J. Water Flow in Carbon Nanotubes: Transition to Subcontinuum Transport. *Phys. Rev. Lett.* **2009**, *102*, 184502.
(36) Corry, B. Designing Carbon Nanotube Membranes for Efficient Water Desalination. *J. Phys. Chem. B* **2008**, *112*, 1427−1434.
(37) Zhang, X.; Zhou, W.; Xu, F.; Wei, M.; Wang, Y. Resistance of Water Transport in Carbon Nanotube Membranes. *Nanoscale* **2018**, *10*, 13242−13249.
(38) Zhou, W.; Wei, M.; Zhang, X.; Xu, F.; Wang, Y. Fast Desalination by Multilayered Covalent Organic Framework (COF) Nanosheets. *ACS Appl. Mater. Interfaces* **2019**, *11*, 16847−16854.
(39) Kang, Y.; Zhang, Z.; Shi, H.; Zhang, J.; Liang, L.; Wang, Q.; Ågren, H.; Tu, Y. Na+ and K+ ion selectivity by size-controlled biomimetic graphene nanopores. *Nanoscale* **2014**, *6*, 10666−10672.
(40) Zhang, L.; Jia, L.; Zhang, J.; Li, J.; Liang, L.; Kong, Z.; Shen, J.-W.; Wang, X.; Zhang, W.; Wang, H. Understanding the Effect of Chemical Modification on Water Desalination in Boron Nitride Nanotubes Via Molecular Dynamics Simulation. *Desalination* **2019**, *464*, 84−93.
(41) Sanz, E.; Vega, C.; Abascal, J.; MacDowell, L. Phase Diagram of Water from Computer Simulation. *Phys. Rev. Lett.* **2004**, *92*, 255701.
(42) Corry, B. Mechanisms of Selective Ion Transport and Salt Rejection in Carbon Nanostructures. *MRS Bull.* **2017**, *42*, 306−310.
(43) Xu, F.; Wei, M.; Zhang, X.; Wang, Y. Ion Rejection in Covalent Organic Frameworks: Revealing the Overlooked Effect of in-Pore Transport. *ACS Appl. Mater. Interfaces* **2019**, *11*, 45246−45255.
(44) Richards, L. A.; Schäfer, A. I.; Richards, B. S.; Corry, B. The Importance of Dehydration in Determining Ion Transport in Narrow Pores. *Small* **2012**, *8*, 1701−1709.
(45) Sahu, S.; Di Ventra, M.; Zwolak, M. Dehydration as a Universal Mechanism for Ion Selectivity in Graphene and Other Atomically Thin Pores. *Nano Lett.* **2017**, *17*, 4719−4724.
(46) Yu, Y.; Fan, J.; Xia, J.; Zhu, Y.; Wu, H.; Wang, F. Dehydration Impeding Ionic Conductance through Two-Dimensional Angstrom-Scale Slits. *Nanoscale* **2019**, *11*, 8449−8457.
(47) Tunuguntla, R. H.; Henley, R. Y.; Yao, Y.-C.; Pham, T. A.; Wanunu, M.; Noy, A. Enhanced Water Permeability and Tunable Ion Selectivity in Subnanometer Carbon Nanotube Porins. *Science* **2017**, *357*, 792−796.

https://dx.doi.org/10.1021/acs.jpcc.0c03641
J. Phys. Chem. C 2020, 124, 20498−20505